Ballistic Transport through a Strained Region on Monolayer Phosphorene *

Yi Ren(任裔), Fang Cheng(程芳)**

Department of Physics and Electronic Science, Changsha University of Science and Technology, Changsha 410004

(Received 12 November 2016)

We investigate quantum transport of carriers through a strained region on monolayer phosphorene theoretically. The electron tunneling is forbidden when the incident angle exceeds a critical value. The critical angles for electrons tunneling through a strain region for different strengths and directions of the strains are different. Owing to the anisotropic effective masses, the conductance shows a strong anisotropic behavior. By tuning the Fermi energy and strain, the channels can be transited from opaque to transparent, which provides us with an efficient way to control the transport of monolayer phosphorene-based microstructures.

PACS: 73.22.−f, 73.63.−b, 68.65.−k DOI: 10.1088/0256-307X/34/2/027302

Recently, layered black phosphorus has attracted intensive attention due to its unique electronic properties and potential applications in nanoelectronics.[1−4] Different from graphene in the electronic band structure, black phosphorus is a semiconductor with a sizeable gap. Phosphorene-based field effect transistors (FETs) show a higher ON/OFF ratio compared with graphene[5,6] and have higher carrier mobility with respect to two-dimensional (2D) transition metal dichalcogenides,[7] which make black phosphorus a favorable material for next-generation electronics. To date, various interesting properties for phosphorene have been predicted, particularly those related to tunable optical properties,[8−11] mechanical anisotropy,[12] and thermal conductivity.[13]

Strain engineering is an efficient mechanical approach to manipulating the physical properties in quasi-2D nanostructures. It has been shown in a number of previews works that mechanical strain is an effective means to generate a finite electronic bandgap for graphene.[14] The in-plane uniaxial strains along the armchair and zigzag directions have also been used to modify the bandgap of black phosphorus.[15,16] First-principles calculations have shown that both biaxial and uniaxial strains rotate the preferred electrical conducting direction by 90°.[17] The method of invariants has been applied to investigate the electronic band structure of black phosphorus with external fields including the strain field.[18] A large uniaxial strain in the direction normal to the black phosphorus plane can even induce a semiconductor-metal transition.[19]

In this Letter, we study the quantum transport of carriers through a strained region on monolayer phosphorene. The tunneling is forbidden when the incident angle exceeds a critical value. The critical angle for electrons tunneling is different for transport along different directions as the different modifications of the bandgap by the x/y strain. The channels can be transited from opaque to transparent by tuning the Fermi energy and strain.

The puckered atomic structure of phosphorene and its geometrical parameters are shown in Fig. 1, where the x and y axes are the armchair and zigzag directions, respectively, and the z axis is in the normal direction to the plane of phosphorene. The components of the geometrical parameters as shown in Figs. 1(a) and 1(b), $(r_{1x}, r_{1y}, r_{1z}) = (1.503, 1.660, 0)$ and $(r_{2x}, r_{2y}, r_{2z}) = (0.786, 0, 2.140)$. The bond lengths are $r_1 = \sqrt{r_{1x}^2 + r_{1y}^2 + r_{1z}^2} = 2.240$ Å, $r_2 = \sqrt{r_{2x}^2 + r_{2y}^2 + r_{2z}^2} = 2.280$ Å, and r_3, r_4 and r_5 are simply defined by parameters of r_1 and r_2. The two in-plane lattice constants are $a = 4.580$ Å, $b = 3.320$ Å and the thickness of a single layer due to the puckered nature is $r_{2z} = 2.140$ Å. The structure parameters have been taken from Ref. [20], which are very close to experimentally measured parameters[21] for its bulk structure.

It has been shown that the bond lengths and bond angles of phosphorene both change under axial strains.[22,23] According to the Harrison rule,[24,25] the hopping parameters for p orbitals are related to the bond length as $t_i \propto 1/r_i^2$ and the angular dependence can be described by the hopping integrals along the π and σ bonds. Though the changes in angles are almost noticeable, the modification of the hopping parameters due to them is much smaller than the effect of changes of bond lengths.[26] Hence, we consider only changes of the bond lengths in the hopping modulation. When an axial strain is applied to phosphorene, the rectangle shape of the unit cell with lattice constants of a_0 and b_0 remains unchanged. Therefore the initial geometrical parameter r_i^0 is deformed as $(r_{ix}, r_{iy}, r_{iz}) = ((1+\varepsilon_x)r_{ix}^0, (1+\varepsilon_y)r_{iy}^0, (1+\varepsilon_z)r_{iz}^0)$, where ε_j is the strain in the j-direction, and r_i is a deformed geometrical parameter. In the linear deformation regime, expanding the norm of r_i to the first order of ε_j gives $r_i = (1+\alpha_x^i\varepsilon_x+\alpha_y^i\varepsilon_y+\alpha_z^i\varepsilon_z)r_i^0$, where $\alpha_j^i = (r_{ij}^0/r_i^0)^2$ are the coefficients related to the structure of phosphorene, which are simply calculated via the special geometrical parameters given above. Using the Harrison relation, we obtain the strain effect on the hopping parameters as

$$t_i \approx (1 - 2\alpha_x^i\varepsilon_x - 2\alpha_y^i\varepsilon_y - 2\alpha_z^i\varepsilon_z)t_i^0. \quad (1)$$

*Supported by the National Natural Science Foundation of China under Grant No 11374002, the Science and Technology Innovative Research Team in Higher Educational Institutions of Hunan Province, and the Construct Program of the Key Discipline in Hunan Province.

**Corresponding author. Email: chengfangg@gmail.com

© 2017 Chinese Physical Society and IOP Publishing Ltd

These hopping parameters are $t_1^0 = -1.220\,\text{eV}$, $t_2^0 = 3.665\,\text{eV}$, $t_3^0 = -0.205\,\text{eV}$, $t_4^0 = -0.105\,\text{eV}$ and $t_5^0 = -0.055\,\text{eV}$.[27]

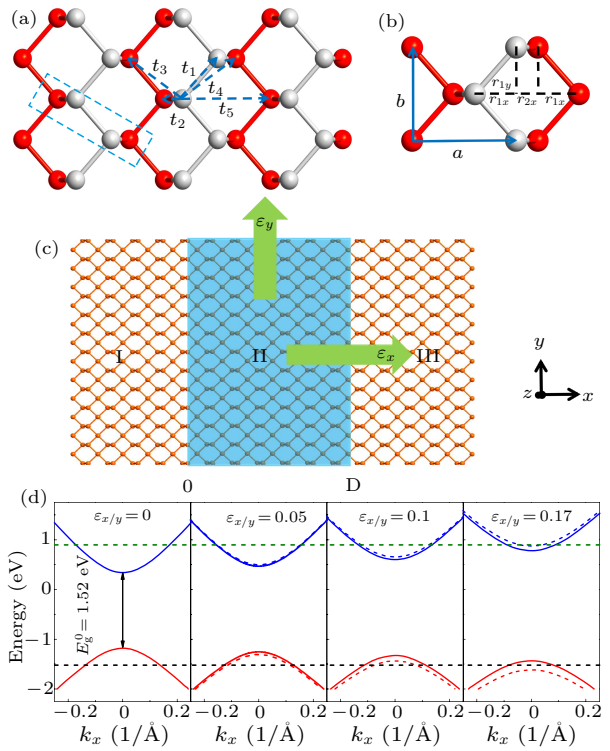

Fig. 1. The lattice geometry of phosphorene. The two different colors of the P atoms refer to upper and lower chains. (a) The hopping parameters $t_1, t_2, \ldots, t_5$ are indicated in the figure. The blue dashed rectangle shows the unit cell of phosphorene. (b) Lattice constants and the components of geometrical parameters describing the structure of phosphorene. (c) Schematic diagram of a strained region geometry on monolayer phosphorene. (d) The energy dispersions of monolayer phosphorene with different strains. The dashed lines indicate the positions of the Fermi energies chosen for the calculations in Fig. 2. The green dashed line is for $E_\text{F} = 0.9\,\text{eV}$, and the black dashed line is for $E_\text{F} = -1.5\,\text{eV}$, respectively.

The spin-orbital coupling (SOC) of the P atom is very small since the atomic SOC is proportional to Z^4, where $Z = 15$ for the P atom. It was shown that the energy gap of a few-layers of black phosphorene can be closed under a huge external electric field or strain.[28,29] However, a topological nontrival energy gap of 5 meV[28] induced by spin-orbital coupling can be opened in few layers of black phosphorene under such a huge electric field. The spin-orbital coupling would not affect the conclusion qualitatively. All P atoms in a unit cell have the same on-site energy, thus we can project the position of upper and lower chains of phosphorene on a horizontal plane to reduce the spinless 4×4 Hamiltonian into a two-band TB model.[10] The new K-space Hamiltonian of the strained phosphorene is given by

$$H = \begin{pmatrix} B_k e^{i(k_a-k_b)/2} & A_k + C_k e^{i(k_a-k_b)/2} \\ A_k^* + C_k^* e^{-i(k_a-k_b)/2} & B_k e^{i(k_a-k_b)/2} \end{pmatrix}, \tag{2}$$

where

$$\begin{aligned} A_k &= t_2 + t_5 e^{-ik_a}, \\ B_k &= 4t_4 e^{-i(k_a-k_b)/2}\cos(k_a/2)\cos(k_b/2), \\ C_k &= 2e^{ik_b/2}\cos(k_b/2)(t_1 e^{-ik_a} + t_3), \end{aligned} \tag{3}$$

with $k_a = \boldsymbol{k}\cdot a$, $k_b = \boldsymbol{k}\cdot b$ and $\theta = \arctan(r_{1y}/r_{1x})$. By expanding the structure factors around $k = 0$ (Γ point) and retaining the terms up to the second order in k, one can write a long-wavelength approximation for the Hamiltonian as

$$H_k = \begin{pmatrix} u_0 + \eta_x k_x^2 + \eta_y k_y^2 & m_{12} \\ m_{21} & u_0 + \eta_x k_x^2 + \eta k_y^2 \end{pmatrix}, \tag{4}$$

where $m_{12} = \delta + \gamma_x k_x^2 + \gamma_y k_y^2 + i\chi k_x$, $m_{21} = \delta + \gamma_x k_x^2 + \gamma_y k_y^2 - i\chi k_x$, $u_0 = 4t_4$, $\eta_x = -\frac{1}{2}a^2 t_4$, $\eta_y = -\frac{1}{2}b^2 t_4$, $\delta = 2t_1 + t_2 + 2t_3 + t_5$, $\gamma_x = -\frac{1}{4}a^2(t_1 + t_3) - \frac{1}{2}a^2 t_5$, $\gamma_y = -\frac{1}{4}b^2(t_1 + t_3)$, and $\chi = -a(t_1 - t_3 + t_5)$. The continuum approximation Hamiltonian can be rewritten in a more compact form as

$$H = \begin{pmatrix} \epsilon_1 & \epsilon_2 e^{i\theta_k} \\ \epsilon_2 e^{-i\theta_k} & \epsilon_1 \end{pmatrix}, \tag{5}$$

where $\epsilon_1 = \frac{F_+ + F_-}{2}$, $\epsilon_2 = \sqrt{(\frac{F_+ - F_-}{2})^2 + (\chi k_x)^2}$, $\theta = \arctan(\frac{2\chi k_x}{F_+ - F_-})$. Here we defined $F_\pm = (u_0 \pm \delta) + (\eta_x \pm \gamma_x)k_x^2 + (\eta_y \pm \gamma_y)k_y^2$. At the Γ point, the F_+ and F_- expressions yield the dispersions for the conduction and valence bands, respectively.

Thus using this polar notation, one can readily obtain the eigenstates as

$$\Psi = \frac{1}{\sqrt{2}} \begin{pmatrix} 1 \\ \lambda e^{-i\theta_k} \end{pmatrix}, \tag{6}$$

where $\lambda = \pm 1$ with the positive (negative) signs corresponding to electrons (holes). Dispersion relations for electrons and holes are then given by

$$\begin{aligned} E = {} & u_0 + \eta_x k_x^2 + \eta_y k_y^2 \\ & \pm \sqrt{(\delta + \gamma_x k_x^2 + \gamma_y k_y^2)^2 + (\chi k_x)^2}. \end{aligned} \tag{7}$$

At the Γ ($k_x = k_y = 0$) point, $E_{(c,v)} = u_0 \pm \delta = 4t_4 \pm (2t_1 + t_2 + 2t_3 + t_5)$. In terms of Eq. (1), we obtain the band gap $E_\text{g} = (4t_1^0 + 2t_2^0 + 4t_3^0 + 2t_5^0) - \sum_j (8\alpha_j^1 \varepsilon_j t_1^0 + 4\alpha_j^2 \varepsilon_j t_2^0 + 8\alpha_j^3 \varepsilon_j t_3^0 + 4\alpha_j^5 \varepsilon_j t_5^0)$, where j denotes the summation over x, y, z components. The first bracket is the unstrained band gap, i.e., $E_\text{g}^0 = 1.52\,\text{eV}$ and the second one indicates the structural dependent values of changes in the band gap due to the axial strains. Inserting the numerical values of the structural parameters to the band gap equation, we obtain $E_\text{g} = E_\text{g}^0 - \sum_j \eta_j \varepsilon_j$, where $\eta_x = -4.09\,\text{eV}$, $\eta_y = -5.73\,\text{eV}$ and $\eta_z = 12.86\,\text{eV}$. For in-plane axial strain, i.e., $\epsilon_x \neq 0$, $\epsilon_y \neq 0$, and $\epsilon_z = 0$, we have the strain-induced modification in the bandgap $E_\text{g} = 1.52 + 4.09\epsilon_x + 5.73\epsilon_y$.

Due to the translation invariance in the y-direction, the solution of Eq. (2) in the jth region can

be written as $\Psi_j(x,y) = \Psi_j(x)\exp(ik_y y)$. We model the stain potential by a step-like potential. This idealized model can give the essential features of the quantum tunneling. A smoother experimentally realizable potential profile would not change the main results. The wavefunctions $\Psi_j(x)$ in the three different regions $x<0$, $0<x<D$ and $x>D$ are written as

$$\Psi_{\rm I} = \frac{1}{\sqrt{2}}\begin{pmatrix}1\\ \lambda e^{-i\theta_0}\end{pmatrix}e^{ik_x x} + \frac{r}{\sqrt{2}}\begin{pmatrix}1\\ -\lambda e^{i\theta_0}\end{pmatrix}e^{-ik_x x},$$
$$\Psi_{\rm II} = \frac{a}{\sqrt{2}}\begin{pmatrix}1\\ \lambda_1 e^{-i\theta}\end{pmatrix}e^{iq_x x} + \frac{b}{\sqrt{2}}\begin{pmatrix}1\\ -\lambda_1 e^{i\theta}\end{pmatrix}e^{-iq_x x},$$
$$\Psi_{\rm III} = \frac{t}{\sqrt{2}}\begin{pmatrix}1\\ \lambda e^{-i\theta_0}\end{pmatrix}e^{ik_x x}, \tag{8}$$

where $\theta = \arctan(k_y/q_x)$,

$$k_y = \sqrt{\frac{(E-u_0^0\mp\delta^0)\tan^2\theta_0}{(\eta_x^0\pm\gamma_x^0\pm\frac{(\chi^0)^2}{2\delta^0})\pm(\eta_y^0\pm\gamma_y^0)\tan^2\theta_0}}, \tag{9}$$

$$q_x = \sqrt{\frac{(E-u_0\mp\delta)-(\eta_y\pm\gamma_y)k_y^2}{(\eta_x\pm\gamma_x\pm\frac{\chi^2}{2\delta})}}, \tag{10}$$

with u_0^0, δ^0, η_x^0, η_y^0, γ_x^0, γ_y^0 and χ^0 being parameters in the absence of the strain. The critical angle is

$$\theta_{\rm c} = \arctan\left(\sqrt{\frac{(\eta_x^0\pm\gamma_x^0\pm\frac{(\chi^0)^2}{2\delta^0})}{\frac{(E-u_0^0\mp\delta^0)}{(E-u_0\mp\delta)}(\eta_y\pm\gamma_y)-(\eta_y^0\pm\gamma_y^0)}}\right). \tag{11}$$

When θ_0 exceeds the critical angle $\theta_{\rm c}$, q_x is purely imaginary.

To obtain the transmission probabilities through a strained region, we calculate the undetermined coefficients through the application of the boundary conditions, i.e., the wavefunctions should be continuous at the interfaces $x=0$ and $x=D$. The transmission probability is obtained as

$$T = \frac{1}{\cos^2(q_x D)+\sin^2(q_x D)\frac{(kk'-\lambda\lambda_1 k_y^2)^2}{k_x^2 q_x^2}}. \tag{12}$$

Note that T is not only a function of the energy but also of the incident angle θ_0 of the incoming carriers.

Based on the obtained results for the transmission probabilities T, one can find the two-terminal Landauer conductance G for the finite structure. Within a linear regime on bias voltage at very low temperatures, the conductance is given by

$$G(E_{\rm F}) = G_0(E_{\rm F})\int_{-\pi/2}^{\pi/2} T\cos\theta_0 d\theta_0, \tag{13}$$

where $G_0 = ge^2E_{\rm F}L_y/(h^2v_{\rm F})$, L_y is the length of the slab in the transverse (y) direction, and g equals 4 due to the transmission probability for spin-up (down) electrons.

The transmission spectra for electrons traversing such a strained region are shown in Fig. 2. For a fixed incident energy $E_{\rm F}=0.9$ eV, the transmission declines sharply and then is blocked when the incident angle exceeds a critical value (see Figs. 2(a) and 2(b)), while the wavevector q_x in the strained region becomes imaginary denoting the appearance of evanescent modes. Comparing Fig. 2(a) with Fig. 2(b), we find that the critical angle is different for the same strength and different directions in-plane strains, which can be understood from Eq. (11). It is interesting to notice that for the same strength strain the critical value $\theta_{\rm c}$ becomes smaller and the tunneling is forbidden for a wider region when the direction of the strain in the Ⅱ region changes from x-direction to y-direction. As is seen, for the incident energy $E_{\rm F}=-1.5$ eV, the strained region becomes transparent at the incident angle $\theta_0=0$ (see Figs. 2(c) and 2(d)). The transmission probability displays a sharp peak at a specific incident angle, i.e., a strong momentum filtering. Here the resonant angles θ_{0m} are determined by $q_x D = m\pi$ ($m=1,2,\ldots$) and $\theta_{0m}\in$Reals. As shown in Figs. 2(c) and 2(d), the resonant angles for $\epsilon_x=0.05$ are different from that for $\epsilon_y=0.05$. The positions and number of resonant peaks are tuned by the strain and the incident energy.

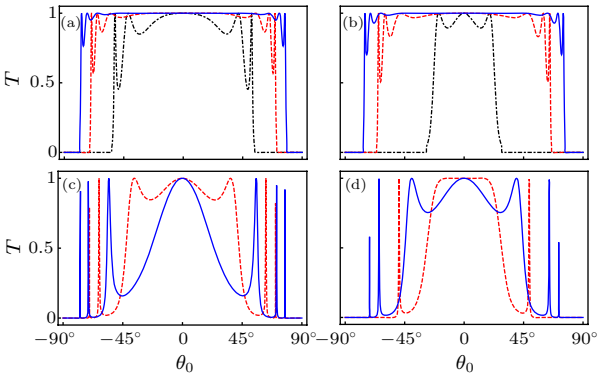

Fig. 2. (Color online) Transmission probability as a function of the incident angle for (a) the incident energy $E_{\rm F}=0.9$ eV and several representative ϵ_x, (b) $E_{\rm F}=0.9$ eV and several representative ϵ_y, (c) $E_{\rm F}=-1.5$ eV and several representative ϵ_x, (d) $E_{\rm F}=-1.5$ eV and several representative ϵ_y. The blue, red dashed and black dot-dashed lines correspond to the results for $\epsilon_{x/y}=0.05$, 0.1 and 0.17, respectively. The width of the strained region is $D=10$ nm.

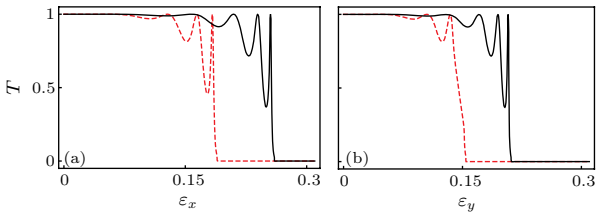

Fig. 3. (Color online) Transmission probability as a function of (a) ϵ_x, (b) ϵ_y for two different incident energies $E_{\rm F}=0.9$ eV (dashed line) and $E_{\rm F}=1.1$ eV (solid line). The incident angle is fixed at $\theta_0=\pi/4$. The width of the strained region is $D=10$ nm.

To show the switching behavior in a strained system more clearly, we plot the dependence of the transmission on the strengths of the in-plane strains in Fig. 3. The in-plane strain shifts the gap by modifying the hopping parameters. A sufficient high in-plane strain switches off the transport when the Fermi energy is the gap in the strained system. The

transmitted channels are blocked at $\epsilon_x \approx 0.19$ or $\epsilon_y \approx 0.15$ for the fixed incident energy $E_{\rm F} = 0.9\,{\rm eV}$ and the incident angle $\theta_0 = \pi/4$. The conduction band edge in the absence of the in-plane strain is $E_{\rm c} = u_0^0 + \delta^0 = 4t_4^0 + (2t_1^0 + t_2^0 + 2t_3^0 + t_5^0) = 0.34\,{\rm eV}$. The conduction band edge in the presence of the in-plane strain in the Ⅱ region is larger than that in the absence of the in-plane strain. The increased values of the conduction band edge for different directions of in-plane strains are different (see Fig. 1(d)). In the vicinity of the gap where the tunneling is forbidden, the critical value of the strain depends sensitively on the direction of the strain. When $k_y > k'$, the longitudinal wave vector q_x in the middle region becomes imaginary, thus transmission is totally blocked. For a given incident angle, a larger Fermi energy corresponds to a larger value of k'. The transverse wave vector k_y is conserved, while the Fermi wavevector is different in Ⅱ and Ⅲ regions as a consequence of strain. Therefore, the critical strength of the strain is larger for a larger Fermi energy. These results are consistent with that in Fig. 2.

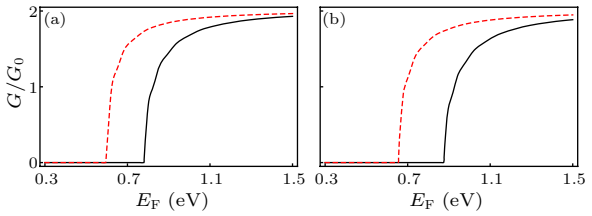

Fig. 4. (Color online) Conductance as a function of the incident energy for several representative strain (a) ϵ_x, and (b) ϵ_y. The red and black dashed lines are for $\epsilon_{x/y} = 0.1$ and 0.17, respectively. The width of the strained region is $D = 10\,{\rm nm}$.

Finally, we plot the conductance versus the Fermi energy for transport through a strained region of width $D = 10\,{\rm nm}$ with strain $\epsilon_{x/y} = 0.1$ (solid line) and $\epsilon_{x/y} = 0.17$ (dashed line) in Fig. 4. The width of the gap in the conductance decreases with the increasing strain. The critical incident energy for a fixed strength of the strain ϵ_x is different from that for a fixed strength of the strain ϵ_y, as the different effective masses along x and y directions. The crossover from the zero to the plateau 2 occurs in a small region of the incident energy $E_{\rm F}$, indicating an electric switching effect.

In summary, we have investigated quantum transport of carriers through a strained region on monolayer phosphorene theoretically. Generally, the transmission probability for transport through such structure declines sharply and then is blocked when the incident angle exceeds a critical value for a fixed incident energy in the conduction band. The critical angle for electrons tunneling is different for transport along different directions as the different modification of the bandgap by the x/y strain. The transmission probability displays a sharp peak at a specific incident angle for a fixed incident energy in the valence band. The positions of resonant peaks depend on the strain and incident energy. The width of the gap in the conductance decreases with increasing the strength of the strains. This feature provides us with an efficient way to control the transport of monolayer phosphorene-based microstructures.

References

[1] Li X, Du Y, Si M, Yang L, Li S, Li T, Xiong X, Ye P and Wu Y 2016 *Nanoscale* **8** 3572
[2] Churchill H O and Jarillo-Herrero P 2014 *Nat. Nanotechnol.* **9** 330
[3] Reich E S 2014 *Nature* **506** 19
[4] Castellanos-Gomez A, Vicarelli L, Prada E, Island J O, Narasimha-Acharya K L, Blanter S I, Groenendijk D J, Buscema M, Steele G A, Alvarez J V, Zandbergen H W, Palacios J J and van der Zant H S J 2014 *Two-Dimensional Mater.* **1** 025001
[5] Koenig S P, Doganov R A, Schmidt H, Castro Neto A H and Özyilmaz B 2014 *Appl. Phys. Lett.* **104** 103106
[6] Li L, Yu Y, Ye G J, Ge Q, Ou X, Wu H, Feng D, Chen X H and Zhang Y 2014 *Nat. Nanotechnol.* **9** 372
[7] Xia F, Wang H and Jia Y 2014 *Nat. Commun.* **5** 4458
[8] Li L, Yang F, Ye G J, Zhang Z, Zhu Z, Lou W, Zhou X, Li L, Watanabe K, Taniguchi T, Chang Kai, Wang Y, Chen X H and Zhang Y 2016 *Nat. Nanotechnol.* **11** 593
[9] Zhang R, Zhou X Y, Zhang D, Lou W K, Zhai F and Chang K 2015 *Two-Dimensional Mater.* **2** 045012
[10] Zhou X, Lou W K, Zhai F and Chang K 2015 *Phys. Rev.* B **92** 165405
Sisakht E T, Zare M H and Fazileh F 2015 *Phys. Rev.* B **91** 085409
Ezawa M 2014 *New J. Phys.* **16** 115004
[11] Nourbakhsh Z and Asgari R 2016 *Phys. Rev.* B **94** 035437
[12] Verma D, Hourahine B, Frauenheim T, James R D and Dumitrică T 2016 *Phys. Rev.* B **94** 121404(R)
[13] Qin G, Zhang X, Yue S Y, Qin Z, Wang H, Han Y and Hu M 2016 *Phys. Rev.* B **94** 165445
[14] Castro Neto A H, Guinea F, Peres N M R, Novoselov K S and Geim A K 2009 *Rev. Mod. Phys.* **81** 109
[15] Elahi M, Khaliji K, Tabatabaei S M, Pourfath M and Asgari R 2015 *Phys. Rev.* B **91** 115412
[16] Jose P S, Parente V, Guinea F, Roldá n R and Prada E 2016 *Phys. Rev.* X **6** 031046
[17] Fei R and Yang L 2014 *Nano Lett.* **14** 2884
[18] Voon L C L Y, Lopez-Bezanilla A, Wang J, Zhang Y and Willatzen M 2015 *New J. Phys.* **17** 025004
[19] Rodin A S, Carvalho A and Castro N A H 2014 *Phys. Rev. Lett.* **112** 176801
[20] Qiao J S, Kong X H, Hu Z X, Yang F and Ji W 2014 *Nat. Commun.* **5** 4475
[21] Takao Y, Asahina H and Morita A 1981 *J. Phys. Soc. Jpn.* **50** 3362
[22] Wang C, Xia Q, Nie Y and Gu G 2015 *J. Appl. Phys.* **117** 124302
[23] Sa B, Li Y L, Qi J, Ahuja R and Sun Z 2014 *J. Phys. Chem.* C **118** 26560
[24] Tang H, Jiang J W, Wang B S and Su Z B 2009 *Solid State Commun.* **149** 82
[25] Harrison W A 1999 *Elementary Electronic Structure* (Singapore: World Scientific Press)
[26] Taghizadeh Sisakht E, Fazileh F, Zare M H, Zarenia M and Peeters F M 2016 *Phys. Rev.* B **94** 085417
[27] Rudenko A N and Katsnelson M I 2014 *Phys. Rev.* B **89** 201408(R)
[28] Liu Q, Zhang X, Abdalla L, Fazzio A and Zunger A 2015 *Nano Lett.* **15** 1222
[29] Zhang T, Lin J H, Yu Y M, Chen X R and Liu W M 2015 *Sci. Rep.* **5** 13927